2016-01-01

# Microstructural Characterization of High Velocity Oxy Fuel Coatings of Inconel 718 and Iron Aluminides

Ana Cecilia Rios Ibanez
*University of Texas at El Paso*, acrios2@miners.utep.edu

# MICROSTURCTURAL CHARACTERIZATION OF HIGH VELOCITY OXY FUEL COATINGS OF INCONEL 718 AND IRON ALUMINIDES

ANA CECILIA RIOS IBANEZ

Master's Program in Mechanical Engineering

APPROVED:

Ahsan Choudhuri, Ph.D., Chair

Ramana Chintalapalle, Ph.D.

Luis Rene Contreras-Sapien , Ph.D.

Charles Ambler, Ph.D.
Dean of the Graduate School

# Dedication

To God and my mom. Even in doubt they knew I would pull this through. To my professors, who gave me the chance and to my friends, for their unmeasurable support.

# MICROSTURCTURAL CHARACTERIZATION OF HIGH VELOCITY OXY FUEL COATINGS OF INCONEL 718 AND IRON ALUMINIDES

by

ANA CECILIA RIOS IBANEZ, B.S. in Mechanical Engineering

THESIS

Presented to the Faculty of the Graduate School of

The University of Texas at El Paso

in Partial Fulfillment

of the Requirements

for the Degree of

MASTER OF SCIENCE

Mechanical Engineering

THE UNIVERSITY OF TEXAS AT EL PASO

August 2016

# TABLE OF CONTENTS

# LIST OF TABLES

# LIST OF FIGURES

# CHAPTER 1

## 1.1- High Velocity Oxy-Fuel Thermal Spray

In industries such as the automobile, marine, aircraft, and the fossil fuel, parts that undergo different environments such as corrosive and high temperature ones, that are harsh for the materials end up in need of often replacement such as advance ultra-supercritical coal-fired (AUSC) boilers, heat engines, steam turbines and gas turbines (Sidhu T, 2005). The operating conditions of such systems require that they are built with materials that not only can work in the previously mentioned high temperature environment, but also have the necessary mechanical properties to undergo, within a reasonable time frame, the operational parameters and have a creep-fatigue resistance. The damage that metals sustain range from temperature related corrosion and wear abrasion. Several causes of this are due to the porosity of the metal and how well they can sustain the thermal stresses and the normal strain while they are under the working loads and conditions. The final results can yield components that fracture in an early estimated time period due to the high temperatures and corrosive environments that weaken the metals.

A solution to avoid the damage done by high temperatures is applying a barrier of a material that has better heat transfer and presents less porosity and thus doesn't let oxide go deeper and produce dislocations in the atoms of the targeted material that it is covering. The name of these kind of barrier are commonly denominated as Thermal Barrier Coating (TBC), which are normally done around pipes. According to Sidhu et al. coatings provide a way to extend the service of the parts being used up to their maximum capabilities and life period by protecting the mechanical properties against corrosion, wear and erosion. Some of the advantages coatings provide for the industries include a high flexibility concerning alloy selection and personalized resistance to corrosion, lower cost than the ones compared to alloyed bulk materials (Sidhu, T, 2005). To be

able to conclude that a coating has a good quality for high temperature applications, Sidky & Hocking (Sidky, PS & Hocking, MG, 1999) describe some criteria points that coatings should meet, as listed below:

- Smooth surface finish
- Resistant to all types of stress such as: impact, fatigue, creep and thermal
- Coating/substrate must be compatible, meaning that there should not be any gross thermal or structural mismatch
- Diffusion rates at the interface must be minimum
- Embrittling phases must be avoided
- Coating must be ductile and develop uniform, adherent, and ductile scale at low rates

A unique kind of TBC uses rocket principles to create a flame that has a temperature high enough to melt powder metal or ceramics and coat the targeted material. Such TBC employs the technique called Thermal Spraying, which is distinguished by spraying the coating material, in the form of rod, wire or powder, to the surface of a substrate and at the same time is being melted by the flame created. The thermal spray was invented by Swiss inventor, Dr. Max Schoop, in early 1900s when he saw his son playing with a toy cannon. The doctor observed that the shots that were fired, upon impact they would stuck to any surface. This develop to the idea that metals when heated up to the melting point and then sprayed to any surfaced could adhere to them and start to build up thus creating a coating. The expansion of thermal spray was in 1970 when the development of thermal plasmas were introduced along with the need of the industry for materials that could withstand high temperatures and wear resistant capabilities were present.

In this particular thesis, investigations of a thermal spray called High Velocity Oxy-Fuel (HVOF) will be presented. This technique has been reported to produce coatings with low porosity

and high adhesion (Sidhu T, 2005), higher hardness, superior bond strength, lower decarburization, and deposit high performance coatings at moderate cost, compared to other available techniques.

In the HVOF process, at the combustion chamber, when both the oxidizer and fuel start the combustion stage, the creation of high pressure and high temperature are presented, consequently producing a supersonic flame, which flows through the nozzle, travels to the barrel section and is capable of melting (or partially melt) (Sidhu T, 2005) the necessary powder metal particles to deposit the coating. The powder travels by means of a carrier gas, up to the barrel section, where the flame of the gun awaits at a typical temperature of 3000 ºC. The semi solid powder particles are impacted into the surface of the substrate with such force that it peens itself (Lillo T, 2008).

Different HVOF thermal spray systems exist with partly different gun designs and capacities. Each gun design currently used can be divided into first, second, and third generations each having differences based on certain fundamental principles and desired outputs (Zhang D, 2003) (Swank WD, 1994). In first and second generation HVOF thermal spray guns, the pressurized burning of gaseous fuel with oxygen is used to produce an exhaust jet traveling at a speed of about 2000 m/s. The main fundamental difference between the first and second generation is the design of the nozzle. In the first generation gun design, there is typically a relatively large combustion chamber and a straight nozzle. For this type of design a maximum sonic velocity can be produced at the nozzle exit (Oksa, Turunen, T, Varis, & and Hannula, 2011). The second-generation type nozzle is based on the ‘de Laval’ nozzle, which enables higher than sonic velocities in the diverging part of the nozzle. Under standard spray conditions, the systems are operated at a power rating of about 100 kW and are capable of spraying about 2 to 3 kg/h of tungsten carbide-cobalt particles. Third generation systems have power ratings ranging from 100 to 300 kW, exhibit

higher chamber pressures ranging from 0.8 to 2.5 MPa, and are capable of spray rates up to about 10 kg/h of tungsten carbide-cobalt particles.

Particle velocity is very important in thermal spray processes; higher velocity results in higher bond strengths, lower porosity, as the particle has less time to cool down at high velocities, thus impacts a substrate in a semi-melted state. The HVOF process is designed around producing these high velocities. The advantages that HVOF has over other thermal spray processes in terms of particle condition (Oksa, Turunen, T, Varis, & and Hannula, 2011) including:

- Lower flame temperature compared with plasma spraying
- More favorable environment due to less oxidizing atmosphere
- Strongly limited reaction and phase transformations
- High compressive residual stress possible
- Strong adhesion to substrates
- High cohesive strength
- High density
- Lower capital cost and ease of use compared to other processes
- Cost/performance ratio are excellent
- More uniform and efficient particle heating due to high turbulence
- Reduced mixing with ambient air once jet and particle leave the gun
- Thicker coatings than with plasma and arc spraying can be produced
- Lower ultimate particle temperatures compared to other processes
- Process can be automated
- Smooth as-sprayed surface finish

- On-site application and repair of components
- Excellent machined surface finish

Table 1.1 summarizes the reasons the HVOF process produces such high quality coatings.

Table 1.1: Benefits of using HVOF coatings (Metco, 2012)

| **Coating Benefit** | **Main Reasons for this Benefit** |
|---|---|
| Higher density (lower porosity) | Higher impact energy |
| Improved corrosion barrier | Less porosity |
| Higher hardness ratings | Better bonding, less degradation |
| Improved wear resistance | Harder, tougher coating |
| Higher bond and cohesive strengths | Improved particle bonding |
| Lower oxide content | Less in-flight exposure time to air |
| Fewer un-melted particle content | Better particle heating |
| Greater chemistry and phase retention | Reduced time at higher temperatures |
| Thicker coatings (per pass & total) | Less residual stress |
| Smoother as-sprayed surfaces | Higher impact energies |

Coatings form different shapes due to the state in which they are melted. When they are in the combustion zone, powder may be completely or partially melted. Whatever state they are in upon impact on the surface of the substrate, the final microstructure is affected by the degree of melting. HVOF coatings present lamellar grain structure due to rapid solidification of small globules flattened upon striking a colder surface at high velocities.

## 1.2- Problem Statement

The research objective of this project was to understand the nickel-based and iron-based coatings for harsh high-temperature, corrosive environments. The coatings of interest were

investigated for their coating characteristics and morphologies when subjected to different operating conditions and process parameters. The characteristics that were studied are structure, morphology and stability of coatings, and the effects of thermal cycling, oxidation degradation and the influence of the complex interaction of coating failures.

## 1.3- Literature Review

In order to be able to validate any study a review of previous investigations must be performed in order to examine their methods and compare their findings. A short summary of literature related to the subject follows below. Generally speaking, good coating quality, with suitable properties, and required performance for specific applications is the goal in producing thermal spray coatings. In order to reach this goal, a deeper understanding of the spray process as a whole is needed.

### 1.3.1- EXPERIMENTAL STUDIES

Experimental studies have focused heavily on microstructure characterization and certain elements of in-flight particle diagnosis. There have been numerous experimental research works related to the characterization of HVOF thermally sprayed coatings of different alloys (Katanoda H, 2011) (Dongmo E, 2008) (Basu & Cetegen, 2008) (Jang, et al., 2006) (Kawakita J, 2006) (Sidhu TS, 2005) (Tang F, 2004) (Bach FW, 2004) (Heath GR, 1997). However, very few works have considered the characterization of coatings and the relevant operating and process parameters. The following sections provide brief review of the earlier studies carried out in this field with special attention to HVOF coating parametric, microstructural and mechanical properties. The literature review of these sections is characterized under three topics which are (i) HVOF spraying

parameters affecting coating quality; (ii) mechanical and chemical properties of HVOF coatings; and (iii) thermal spray powder characterizations.

### 1.3.2- HVOF Spraying Parameters Affecting Coating Quality

Many variables could affect metallic coating properties, particularly unmelted particles and oxidation level. Flame parameters such as equivalence ratio, velocity (Mach number), and temperature, are very important. Only one study has been published for the most widely used JP5000 Praxair gun (Tabbara H, 2009). In the study sufficient information about the combustion processes and associated complex flow processes of the thermal spray system was not presented.

The combination of computation and physical investigation has seldom been encountered in this subject. Gourlaouen studied stainless steel substrates to address the influence of the spray variables on the coating characterization (Goulaouen, 1998). He concluded that the influence of the combustion temperature was small. On the other hand, an increase of the flame power led to higher the oxidation with low unmelted particles rates and the deposition efficiency was improved. Among the three parameters studied, the equivalence ratio had significant influence. The increase of the equivalence ratio, decreases the oxygen content, and consequently of the microhardness. Also, the increase of the number of unmelted particles resulted in a decrease of the deposition efficiency.

Lillo et al. assured that conditions of quenching, peening and CTE mismatch stresses combined are necessary to have an estimate of residual stress state. This stress state found in the coating can range from compressive, tensile or neutral. Most importantly the resulting stresses are controlled by the pressure chamber of the combustion when the HVOF thermal spray is detonated

(Lillo T, 2008). The study suggests that a compressive stress state is the most desirable result, since tensile stress stimulate cracking propagation in the coatings.

Wei et al. (W.C. Lih, 2000) examined the effect of HVOF spray condition on molten particle velocity and surface temperature. He used carbide/nickel-chromium alloy as a coating powder. He studied oxygen to fuel ratio, fuel gas flow rate, powder carrier gas flow rate, powder feed rate, gun barrel length, stand-off distance and substrate surface speed. The microstructure and mechanical properties of the coating were examined. He concluded that the feed stock rate, standoff distance and gun barrel length played a main role in the output temperature of the molten particle. In addition, he said that sufficient enhancement in abrasion wear resistance was observed by depositing coating at higher particle velocity. He mentioned that coating deposited by molten particles that were heated at high temperatures, ranging from 1650 ºC to 1725 ºC, showed lower porosity content of the coating.

Kuroda et al. investigated the relationship between the conditions of sprayed particles and the stress generated during deposition (S. Kuroda, 2001). They used 316 L stainless steel for both the sprayed powder and the substrates to eliminate the stress due to difference in thermal expansion. They examined different powder sizes and particles velocities to control the kinetic energy. They found that a strong negative correlation existed between the temperature and diameter. In contrast, the correlation was very weak between the diameter and the velocity. They concluded that the process of the stress generation of the HVOF coating was more complicated compared to conventional thermal spray processes because of the peening action of the particles. Their results revealed that a broad window for the stress control was available through the control of spray parameters with the HVOF process.

Totemeier et al. investigated the effects of HVOF spray parameters on spray particle characteristics, deposition efficiency, and residual stresses (T.C. Totemeier, Residual Stresses in

High Velocity Oxy-Fuel Metallic Coatings, 2004). They tested Fe3Al and AISI type 316 stainless steel coating materials. They studied three different spray conditions for each material; the spray particle characteristics (size, distributions, velocity) were assessed for each material and spray condition. They found that increasing torch chamber pressure resulted in increasing spray particles velocity with little change in the spray particles' temperature. Also, relative deposition efficiencies were maximized at an intermediate particle velocity. They mentioned that residual stresses in coating on thin substrates became slightly less compressive with increasing coating thickness.

Zhao et al. (L. Zhoa, 2004) investigated the effect of spray conditions on the particle in flight properties and the properties of HVOF coating of WC-CoCr. The particle size distribution of WC-CoCr powder was -45/+11 μm. They evaluated the microstructure, hardness and wear behavior of the coatings. Their results indicated that the particle and coating characterizations reached different levels because of spray parameters such as the total gas flow rate, the powder fees rate and standoff distance. They concluded that high particle velocity and high particle temperature were caused by increasing the total gas flow rate and lowering the powder feed rate with a short standoff distance. Also, they reported that the particle velocity showed more sensitivity to spray parameters than the particle temperature. In addition, increasing the particle temperature and velocity led to enhancing the coating hardness and decreasing the porosity. They mentioned that the total gas flow rate is more effective parameter than powder feed rate, which had more effect than standoff distance.

Hasan et al. (M. Hasan, 2008) studied the influence of the spray variables on residual stress buildup of HVOF functionally graded coatings. They illustrated that many parameters could affect the residual stress generated on the obtained coating, such as equivalence ratio and spray distance. They concluded that the spray distance had significant influence on the residual stress. Its increase

led to increase the flight time of the particles which in turn, lower the impact velocity and temperature.

### 1.3.3- MECHANICAL AND CHEMICAL PROPERTIES OF HVOF COATINGS

Few current investigations have analyzed substrate coating features based on equipment design characteristics; those examinations focused on coating properties have done that by employing industry-supplied HVOF guns. Physical and mechanical properties of HVOF spray coatings can be analyzed through failure testing such as cyclic loading and performance under high temperature conditions (Jang HJ, 2006). Final coating characteristics may also be analyzed in a Scanning Electron Microscope (SEM) (Tang F, 2004) for detailed visuals on porosity and composition.

Jang et al. (Jang H. P., 2006) studied Co-Ni alloy coatings on a nickel-based super-alloy substrate. In this investigation mechanical properties such as hardness 'H' and modulus of elasticity 'E' were studied as a function of the thickness of the bond coat, as these values are essential in improving reliability and lifetime performance for thermal environments. In their results, the interface between the HVOF applied bond coat and substrate showed a relatively continuous microstructure, with the bond coat appreciated to be quite dense (Jang, et al., 2006); on the other hand, those samples prepared by the Atomic Plasma Spray (APS) process showed slight cracking. Additionally, the thermally grown oxide (TGO) layer formed during fatigue tests tended to increase as a function of temperature and dwell time, but was found to be independent of applied bond coat thickness.

Padilla et al. (K. Padilla, 2002) conducted an experiment in order to study the effect of Ni-5 Mo-5.5 Al (wt. %) applied by HVOF, on the fatigue properties of AISI 4140 steel. The

investigation was carried out by comparing the fatigue behavior of uncoated samples with those of the specimens after grit blasting and after blasting and coating with such a deposit. They carried out tensile and fatigue tests. They concluded that grit blasting gave rise to a significant decrease in the fatigue properties of the material. Further coating of the grit blasted samples, applied by HVOF, led to a further reduction in the fatigue strength of the material. They suggested that such a further decrease was mainly associated with two different causes. First, the extensive fracture and delamination of the coating from the substrate had been observed from the microscopic analysis. Secondly, the possible existence of tensile residual stresses in the substrate, in the vicinity of the substrate deposit interface which would assist in the propagation of the fatigue cracks nucleated at the alumina particles.

Stoica et al. (V. Stoica, 2004) investigated the sliding wear behavior of as sprayed and Hot Isostatically Pressed (HIPed) thermal spray cermet coating deposited by HVOF. They sprayed WC-12C coating powder on bearing steel substrate followed by HIPed at 850ºC. They characterized the coating using X-Ray Diffraction (XRD), Scanning Electron Microscope (SEM) and microhardness test. They concluded that a sufficient enhancement of thermal spray cermet coating wear resistance was observed by hot isostatic pressing post treatment where this offered about 100% improvement in wear behavior of cermet coatings. This enhancement in physical characterizations was due to the phase transformations where secondary phase W2C and metallic tungsten were eliminated.

Wielage et al. (B. Wielage, 2006) carried out two studies in order to develop a HVOF thermal spray system. Firstly, they conducted a study to evaluate the wear behavior of cermet coating deposited on light weight material parts subjected to dynamical load. The second study, using advanced HVOF gun with high combustion chamber pressure to reduce the particle

temperature was investigated. This was because that the cheap belt grinding could be used to finish the former coating. They concluded that HVOF cermet coatings applied on light weight material showed an excellent wear behavior without detraction of fatigue strength. Also, nickel or iron base coating deposited by high combustion pressure had high corrosion resistance due to high density and low oxy-gen content in the coating.

### 1.3.4- COATING POWDER CHARACTERIZATIONS

Tan et al. (J. Tan, 1999) studied the repair of worn components using HVOF thermal spray. They used stainless steel as coating material as well as substrate to restore the worn parts to their original dimensions. They found that HVOF thermal spraying process could be extremely useful as an excellent technique to repair and restore damages with various depths in 2D tool steel substrates. Also, the thickness of 5.5 mm could be achieved if the properties of the coating material with the substrate material were matched. They concluded that WC-Co wasn't an appropriate selection to be used in such repairs.

Reisal et al. (G.Reisel, 2001) investigated the oxidation of unreinforced and reinforced molybdenum disilicade (MoSi2) coatings. The samples were subjected to high temperature 5000ºC, 1000 ºC and 1500 ºC. They used Scanning Electron Microscopy (SEM), Energy Dispersive X-Ray analysis (EDX) and X-Ray Diffraction analysis (XRD) to evaluate the coating characterization. In addition, they employed simultaneous thermo gravimetric equipment to study the oxidation behavior. They noticed that the porosity of the coating had a gradual effect on the pesting reaction of the MoSi2 at 500 ºC. At 1000 ºC, the tests showed that no effect was observed of the heating rate on the short term oxidation properties. At 1500 ºC, they reported that a protective SiO2 layer was formed with a thickness of 10 μm for the unreinforced MoSi2 coating.

Hu et al. (W. Hu, 2008) studied the properties of NiAl nanostructured coating produced by HVOF spraying. Ni and Al compound powder in the atomic ratio 50:50 were melded under Argon gas atmosphere. They used XRD, SEM coupled with EDS to examine the coating properties. They reported that increasing the milling time, reduced the grain size of the powder and increased the lattice constant. They found that HVOF thermal spraying of milled metallic powder was effective for producing Ni Al nanostructure coatings. They found that micro-hardness, dynamic hardness and elastic modulus of the coating decreased as heat treatment increased. In addition, they figured out that increasing temperature led to a decrease in the high temperature hardness.

### 1.3.5- INCONEL 718

During the study of Sidhu et al. Nickel based coatings mixed with chromium were chosen for the reason that when subjected to oxidation, chromium creates a protective surface of Cr2O3 at environments up to 1473K. (Sidhu, 2005). The high resistance to high temperature oxidation and corrosion of the material is used to prevent the concentration of hot gages, molten ashes found in fuel fired boilers and electric furnaces.

Sundararanjan et al subjected its coatings to a steam oxidation testing on temperatures ranging from 600-750C. The tests yield that thick and dense HVOF coating performed better against the steam oxidation, compared to the coatings crated by APS. Once again the creation of Cr2O3 was observed even though it has a low concentration in the coating previous the steam oxidation. It is stipulated that the diffusion of nickel and iron are almost similar.

### 1.3.6- IRON ALUMINIDE

Iron Aluminides coatings, according to Lillo at al. (Lillo T, 2011) most frequently fail due to cracking, delamination or spalling, rather than by corrosion, since the material has a good resistance on a combustion atmosphere fueled by fossil. In this study, the iron aluminide coatings

were subjected to thermal cycling. They concluded that the substrates with small temperature increases presented a greater durability despite that arguing earlier that CTE mismatch would contribute to cracking. Additionally substrate-coatings with the greatest CTE mismatch performed better at the thermal cycling. Ultimately the Iron Aluminide coatings performed well in thermal cycling up to 900C.

# CHAPTER 2: COATING CREATION

## 2.1- HVOF Design

In this section, all components of utilized HVOF thermal spray system and methodologies are presented including the injector, combustion chamber, converging-diverging nozzle, barrel, and cooling jacket. In addition, this section includes the design equations, considerations, and technical issues. The foregoing design calculations provide the dimensions, thicknesses, and orifice sizes for the major components of a gas-fueled HVOF thermal spray gun. Figure 3.1 shows the completed schematic for the newly designed HVOF thermal spray gun.

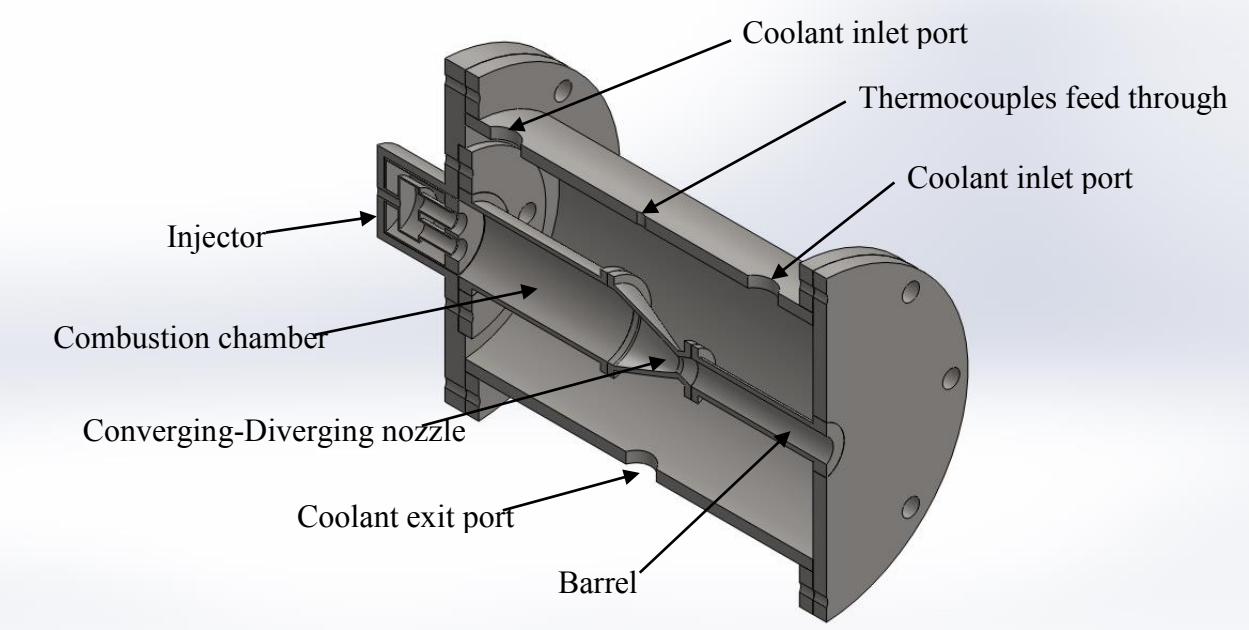


Figure 2.1: 3-D cross-sectional schematic of the current HVOF thermal spray gun

### 2.1.1- INJECTOR

The function of the injector is to introduce the propellants into the combustion chamber in such a way that efficient combustion can occur. The utilized HVOF thermal spray gun in this study employs a shear co-axial injector in which oxidizer and gas fuel are fed under pressure from tanks into a combustion chamber. The propellants consist of gaseous methane along with oxidizer which for current experiments is gaseous oxygen. In the employed HVOF thermal spray gun, the main fuel line is divided into two lines right before the injector face. The first fuel line is partially premixed with the oxidizer line due to the existence of a small recess length between fuel and oxidizer orifices. The subsequent mixture is then injected into the combustion chamber through three even peripherally distributed orifices from the gun centerline. This design was selected since it would enhance mixing between the fuel and oxidizer. A detailed image of the injector system can be seen in Fig. 2.2.

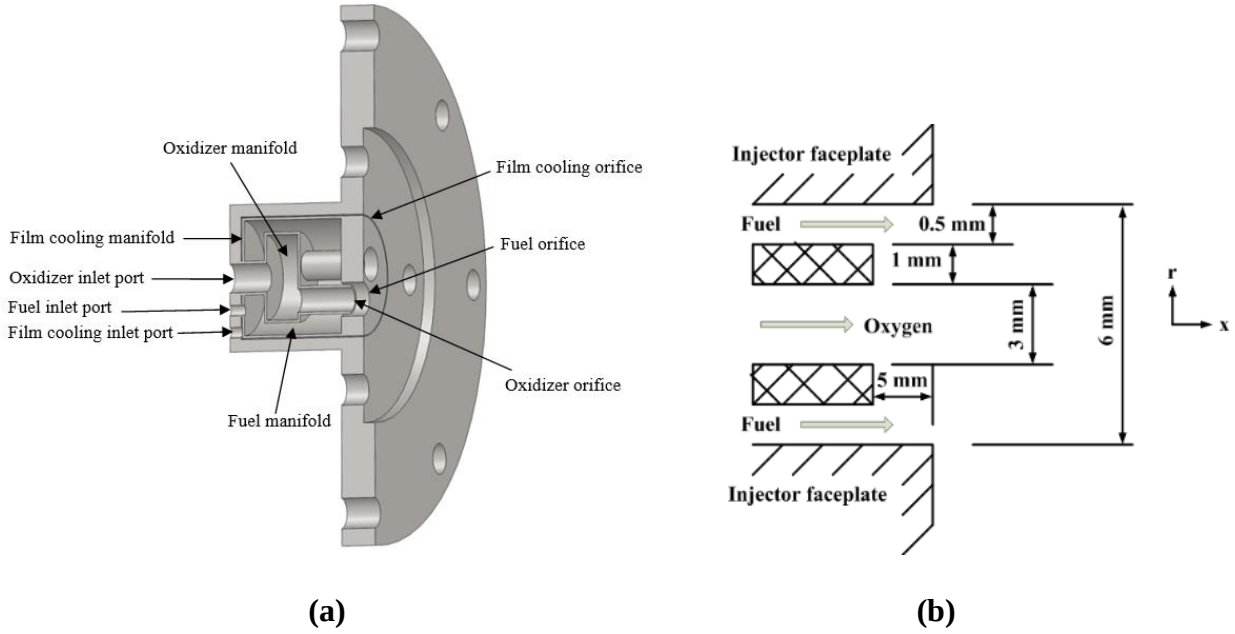


Figure 2.2: a) 3-D Schematic of the utilized shear co-axial injector, b) Schematic diagram of one orifice in the shear co-axial injector used for experiments

Since the fuel burning with oxygen near the stoichiometric equivalence ratio involves very high flame temperatures, a second fuel line enters the injector via a separate port and is injected through a special orifice, close to the chamber wall, to provide the chamber with a film of gas fuel to protect exposed combustion chamber wall surfaces. Film cooling protects the walls from excessive heat and lowers the mixture ratio of any errant streak.

Mass flow rates of total fuel and oxidizer can be calculated assuming the exhaust gas products are in gaseous form. The equations used for the calculation of mass flow rate in the nozzle are from perfect gas law theory seen in Eqs. (1-6) (Huzel, 1992). These equations were used primarily to determine total propellants mass flow rate assuming the nozzle throat diameter is determined at the beginning of the design procedure.

$$\dot{m_t} = \frac{A_t * P_c}{\pi} * \sqrt{\frac{\gamma * g}{R * T_c} * \left[\frac{2}{\gamma + 1}\right]^{\frac{\gamma+1}{\gamma-1}}} \tag{1}$$

$$A_t = \frac{\pi D_t^2}{4} \tag{2}$$

$$R = \frac{\bar{R}}{M_{wt}} \tag{3}$$

$$\dot{m_t} = \dot{m_o} + \dot{m_f} \tag{4}$$

$$\dot{m_o} = \frac{\dot{m_t} * {}^{O}/_{F}}{({}^{O}/_{F} + 1)} \tag{5}$$

$$\dot{m_f} = \frac{\dot{m_t}}{({}^{O}/_{F} + 1)} \tag{6}$$

Where $\dot{m_t}$ is the total propellants mass flow rate, $A_t$ is the cross section area at nozzle throat, $D_t$ is the throat diameter, $P_c$ is the combustion chamber pressure, $\gamma$ is the ratio of gas specific

heats, g is the gravitational acceleration, R is the gas constant, $\overline{R}$ is the universal gas constant, $M_{wt}$ is the gas molecular weight, $T_c$ is the propellants adiabatic flame temperature in combustion chamber, $\dot{m}_o$ is the oxidizer mass flow rate, $\dot{m}_f$ is the fuel mass flow rate, and $O/F$ is the oxygen to fuel ratio.

Based on the output of Eqs. (1-6), injector orifices dimensions can be calculated from Eqs. (7-12) (Sutton, 2005).

$$A_f = \frac{\dot{m}_f}{N * C_d * \sqrt{2 * g * \rho_f * \Delta P_f}} \tag{7}$$

$$A_o = \frac{\dot{m}_o}{N * C_d * \sqrt{2 * g * \rho_o * \Delta P_o}} \tag{8}$$

$$\rho_f = \frac{P_f * \rho_{f_{atm}}}{P_{atm}} \tag{9}$$

$$\rho_o = \frac{P_o * \rho_{o_{atm}}}{P_{atm}} \tag{10}$$

$$P_f = P_c + \Delta P_f \tag{11}$$

$$P_o = P_c + \Delta P_o \tag{12}$$

Where $A_f$ is the fuel orifice cross section area, $A_o$ is the oxidizer orifice cross section area, N is the number of orifices; $\Delta P_f$ is the injection pressure drop in the fuel line, $\rho_f$ is the fuel density, $\rho_{f_{atm}}$ is the fuel density at atmospheric conditions, $\rho_{o_{atm}}$ is the oxidizer density at atmospheric conditions, $C_d$ is a dimensionless discharge coefficient; $\Delta P_o$ is the injection pressure drop in the oxidizer line, $\rho_o$ is the oxidizer density, $P_f$ is the total pressure load in the fuel line, and $P_o$ is the total pressure load in the oxidizer line.

The discharge coefficient is a function of injector orifice configuration. This value ranges from 0.5 to 0.92 and can be determined accurately by experimental means (Sutton, 2005) (Huzel,

1992). For a given injection velocity, a higher value of discharge coefficient results in a lower injection pressure drop. The injection pressure drop must be high enough to eliminate combustion instability inside the combustion chamber but must not be so high that the run tank and pressurization system used to supply fuel and oxygen to the gun are penalized (Huzel, 1992). These values were also taken into consideration during the design of the injection system.

### 2.1.2- COMBUSTION CHAMBER

In order for the fuel and oxygen mixture to chemically react/burn to form hot gases, the chamber must be of sufficient length (Yang V, 2005). A parameter describing the chamber volume required for complete combustion is the characteristic chamber length, which is given by Eq. (13).

$$L^* = \frac{V_c}{A_t} \tag{13}$$

Here $L^*$ is the characteristic chamber length, and $V_c$ is the combustion chamber volume. The combustion chamber volume, $V_c$, includes the volumes of the chamber and the converging section of the nozzle (Huzel, 1992). To reduce losses due to flow velocity of gases within the chamber, the combustion chamber cross-sectional area should be at least three times the nozzle throat area (Sutton, 2005). Additionally, the chamber diameter for small combustion chambers should be three to five times the nozzle throat diameter so the injector will have useable face area (Huzel, 1992).

Chamber volume may be calculated from Eq. (14) assuming combustion chamber length and convergent nozzle half angle are known. A good value for the nozzle convergence half-angle, $\beta$, is from 20° to 45°; however, the nozzle divergence half-angle, $\alpha$, should be no greater than 15° to prevent nozzle internal flow losses (Huzel, 1992), Fig. 2.3.

$$V_c = A_t \left[ \frac{L_c * A_c}{A_t} + \frac{1}{3}\sqrt{\frac{A_t}{\pi}} * Cot\,\beta \left( \left( \frac{A_c}{A_t} \right)^{\frac{1}{3}} - 1 \right) \right] \quad (14)$$

In Eq. (14) $A_c$ is the combustion chamber cross section area, $\beta$ is the convergent nozzle half angle, and $L_c$ is the combustion chamber length.

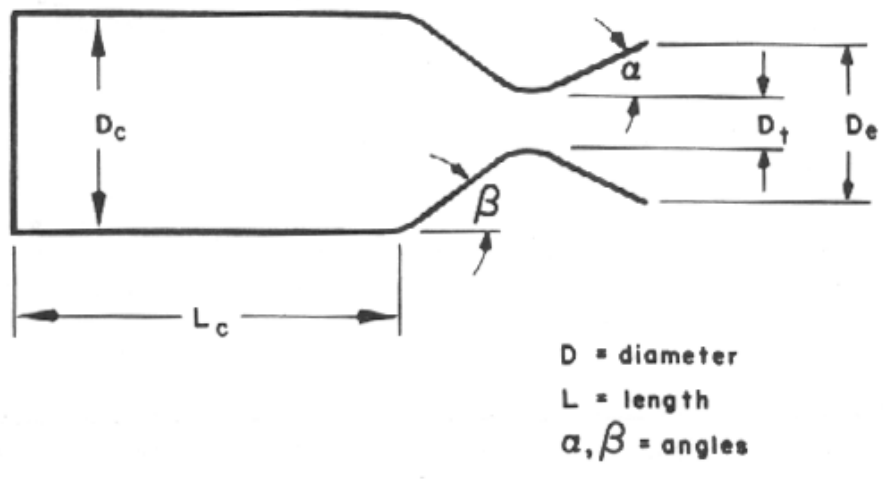


Figure 2. 3: Schematic of geometric parameters in a converging-diverging nozzle attached to combustion chamber

In addition to geometrical considerations, the chamber must be strong enough to contain the high pressures and temperatures generated by the combustion process. In the current design the combustion chamber must be physically attached to the cooling jacket hence chamber wall thicknesses must be sufficient for welding and brazing purposes. Considering the chamber as a cylindrical shell, the chamber wall thickness was computed using Eq. (15) (Sutton, 2005). The chamber wall thickness should be somewhat greater to allow for welding, buckling, and stress concentration. In the current design a safety factor greater than one was used for the calculation of wall thickness. It was determined that the wall thickness of the combustion chamber wall, nozzle, and barrel section are equal (Yang V, 2005).

$$t_w = \frac{P_c * D_c}{2 * S} * \text{safety factor} \quad (15)$$

In Eq. (15) $t_w$ is the chamber wall thickness, $D_c$ is the chamber diameter, and S is the allowable working stress of chamber material.

### 2.1.3- CONVERGING-DIVERGING NOZZLE

The function of the nozzle is to convert the chemical/thermal energy generated in the combustion chamber into kinetic energy. The flow velocity through a nozzle increases to sonic velocity at the throat and then develops supersonically in the diverging section. The nozzle converts the slow moving, high pressure, high temperature gas in the combustion chamber into high velocity gas of lower pressure and temperature (Sutton, 2005). Since thrust or exhaust output of the system is the product of mass and velocity, a very high gas velocity is desirable for the current application. Nozzles, which perform this process, are referred to as de Laval nozzles and consist of a convergent and divergent section, as shown in Fig. 2.4.

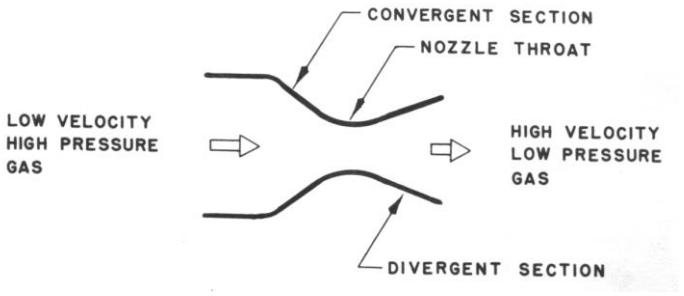


Figure 2. 4: Schematic of a converging-diverging nozzle

For design purposes and simplicity it is assumed that flow through a nozzle is an isentropic expansion process, and that both the total temperature and the total pressure remain constant throughout the nozzle (Huzel, 1992). The static pressure at a nozzle throat with sonic flow, where the maximum mass flow per unit area occurs, is defined as the critical pressure (Yang V, 2005). The velocity of sound is equal to the velocity of propagation of a pressure wave within a medium.

It is, therefore, impossible for a pressure disturbance downstream of the nozzle throat to influence the flow at the throat or upstream of the throat, provided that this disturbance will not create a higher throat pressure than the critical pressure (Sutton, 2005). It is one of the characteristic features of an attached diverging or de Laval nozzle, however, that sonic velocity in the nozzle throat is maintained even if the backpressure at the nozzle exit is greater than the pressure required at the throat for sonic velocity. As a result, a pressure adjustment must take place between the throat and the nozzle exit. This adjustment may take place through subsonic deceleration, or by way of non-isentropic discontinuities called shock waves, or by a combination of both. The flow area at the end of the divergent section is called the nozzle exit area. For the experimental design the temperature and pressure at the nozzle throat was calculated from Eqs. (16 -17).

$$T_t = T_c \left[ \frac{1}{1 + \frac{\gamma - 1}{2}} \right] \tag{16}$$

$$P_t = P_c \left[ 1 + \frac{\gamma - 1}{2} \right]^{\frac{-\gamma}{\gamma - 1}} \tag{17}$$

In these equations $T_t$ is the temperature at nozzle throat, and $P_t$ is the pressure at nozzle throat. The gas Mach number, velocity, and temperature at the nozzle exit were calculated for the current design from Eqs. (18-20) assuming the perfect gas law expansion expression (Huzel, 1992).

$$M_{a_e} = \sqrt{\frac{2}{\gamma - 1} \left[ \left( \frac{P_c}{P_{atm}} \right)^{\frac{\gamma - 1}{\gamma}} - 1 \right]} \tag{18}$$

$$V_e = \sqrt{\frac{2 * g * \gamma * R * T_c}{\gamma - 1} \left[ 1 - \left( \frac{P_{atm}}{P_c} \right)^{\frac{\gamma - 1}{\gamma}} \right]} \tag{19}$$

$$T_e = T_t \left(\frac{P_{atm}}{P_t}\right)^{\frac{\gamma-1}{\gamma}} \tag{20}$$

Where $M_{a_e}$ is the Mach number at nozzle exit, $V_e$ is the gas velocity at nozzle exit, $T_e$ is the gas temperature at nozzle exit, and $P_{atm}$ is the atmospheric pressure.

The nozzle exit cross section area corresponding to the exit Mach number is given by Eq. (21) (Huzel, 1992).

$$A_e = \frac{A_t}{M_{a_e}} \left[ \frac{1 + \frac{\gamma - 1}{2} M_{a_e}^2}{\frac{\gamma + 1}{2}} \right]^{\frac{\gamma+1}{2(\gamma-1)}} \tag{21}$$

Here $A_e$ is the nozzle exit cross section area.

### 2.1.4- BARREL

Powder particles can either be fed through the oxidizer stream or at some location downstream. The former has several disadvantages including particle overheating, wrongful deposition and deposition inside the configuration; nevertheless, it also solves the question on how to effectively introduce seeding powder into a HVOF system. In order to decrease the possibility of overheating and introduce particles directly to supersonic flow most gun configurations inject particles into the barrel through a tapping angle. The barrel has been designed as the section where particle injection occurs and products exit the configuration. Although this section is responsible for controlling and optimizing coating properties, there currently exist no quantitative methods to determine the optimal length. Thus a wide range of experimental tests are being done in order to optimize the effectiveness of the system and will be presented in future works.

### 2.1.5- COOLING JACKET

The average heat transfer rate per unit area in the combustion chamber during the oxy-combustion process is about 6 $MW/m^2$ (Sutton, 2005). It is therefore necessary to implement a cooling system on the combustion chamber to avoid material failure (Yang V, 2005). In total, the largest part of the heat transferred from the hot chamber gases to the chamber walls is attributed to convection, with heat transferred by conduction and radiation comprising approximately 25% of the total heat transfer (Yang V, 2005).

The cooling jacket consists of an inner and outer wall. The combustion chamber forms the inner wall with another concentric but larger cylinder forming the outer wall. The space between the walls serves as the coolant passage. The injector under normal operation is self-cooled by the incoming flow of propellants. The combustion chamber, nozzle, and barrel however require additional cooling for longer duration periods of operation. Of particular importance is the nozzle throat region which because of the smaller geometry is exposed to a very high heat flux (Yang V, 2005). To cool this section of the system an advanced ethylene glycol formula, Dynalene (HC-10), is used because of its ability to absorb heat (Dynalene, n.d.), Table 2.

Table 2.1: Properties of Dynalene (HC-10)

| **Properties** | **Units of measure** |
|---|---|
| Temperature range | 263 to 491 K |
| Specific Heat capacity | 3.28 kJ/kg.K |
| Density | 1200 $kg/m^3$ |

The total heat transferred from the gun to the coolant can be calculated from Eqs. (22-24) assuming the area of the nozzle cone up to the throat to be 10% of the chamber surface area (Huzel, 1992).

$$Q_{total} = q * A_{total} \tag{22}$$

$$A_{total} = \pi * L_c(D_c + 2 * t_w) + area\ of\ nozzle\ cone + \pi * L_{barrel}(D_{barrel} + 2 * t_w) \tag{23}$$

$$A_{total} \cong 1.1 * \pi * L_c(D_c + 2 * t_w) + \pi * L_{barrel}(D_{barrel} + 2 * t_w) \tag{24}$$

Where $Q_{total}$ is the total heat transferred, $q$ is the average heat transfer rate per unit area of a HVOF thermal spray gun, assumed to be 6 MW/m$^2$ (Sutton, 2005), $A_{total}$ is the total heat transfer area, $L_{barrel}$ is the barrel length, and $D_{barrel}$ is the barrel diameter.

The coolant mass flow rate can be calculated by assuming a desired temperature rise of the coolant from Eq. (25):

$$\dot{m}_{coolant} = \frac{Q_{total}}{C_{p_{coolant}} * (T_o - T_i)_{coolant}} \tag{25}$$

Where $\dot{m}_{coolant}$ is the coolant mass flow rate, $C_{p_{coolant}}$ is the specific heat of coolant, $T_o$ is the temperature of coolant leaving jacket, and $T_i$ is the temperature of coolant entering jacket.

The annular flow passage between the combustion chamber wall and the outer jacket must be sized so that the flow velocity of the coolant is at least 10 m/s (Yang V, 2005). The flow passage dimensions can be calculated from Eqs. (26-28) (Huzel, 1992).

$$A_{cooling\ jacket} = \frac{\dot{m}_{coolant}}{\rho_{coolant} * V_{coolant}} \quad (26)$$

$$A_{cooling\ jacket} = \frac{\pi}{4}(D_o^2 - D_i^2) \quad (27)$$

$$D_i = D_c + 2 * t_w \quad (28)$$

Where $A_{cooling\ jacket}$ is the cooling jacket cross section area, $\rho_{coolant}$ is the coolant density, $V_{coolant}$ is the coolant average flow velocity, $D_i$ is cooling jacket inner surface diameter, and $D_o$ is cooling jacket outer surface diameter.

## 2.2- Combustion Parameters

### 2.2.1- Gas-Fueled HVOF Thermal Spray Gun Design

Table 2.2 summarizes all operating conditions and geometric parameters used in the design of the current gas-fueled HVOF thermal spray gun. The present HVOF thermal spray gun was designed to generate gas with velocity up to 1690 m/s, Mach number up to 1.9, and temperature up to 2475 K. The combustion chamber pressure of 700 kPa was selected as a typical condition representative in most commercial HVOF thermal spray guns. After system assembly, component testing was done to ensure the functionality of the system.

Table 2.2: Summary of operating conditions and geometric parameters

| **Inputs** | | **Outputs** | |
|---|---|---|---|
| Oxidizer | Oxygen | Oxidizer mass flow rate, $\dot{m}_o$ | 0.062 kg/s |
| Fuel | Methane | Fuel mass flow rate, $\dot{m}_f$ | 0.018 kg/s |
| Oxygen to fuel ratio, $O/F$ | 3.5 | Total mass flow rate, $\dot{m}_t$ | 0.080 kg/s |
| Ratio of gas specific heats, $\gamma$ | 1.2 | Gun wall thickness, $t_w$ | 5 mm |
| Gas molecular weight, $M_{wt}$ | 26.7 g/mol | Combustion chamber volume, $V_c$ | $2.6*10^{-4}$ $m^3$ |

| | | | |
|---|---|---|---|
| Oxidizer density at $P_{atm}$, $\rho_{o_{atm}}$ | 1.33 kg/m$^3$ | Chamber characteristic length, $L^*$ | 1.49 m |
| Fuel density at $P_{atm}$, $\rho_{f_{atm}}$ | 0.69 kg/m$^3$ | Gas temperature at nozzle exit, $T_e$ | 2475 K |
| Discharge coefficient, $C_d$ | 0.75 | Gas velocity at nozzle exit, $V_e$ | 1690 m/s |
| Number of injector orifices, $N$ | 3 | Gas Mach number at nozzle exit, $M_{a_e}$ | 1.9 |
| Combustion chamber pressure, $P_c$ | 700 kPa | Converging nozzle inlet diameter | 50 mm |
| Combustion chamber adiabatic flame temperature, $T_c$ | 3350 K | Diverging nozzle exit diameter | 21 mm |
| Allowable working stress of stainless steel (SS-316), $S$ | 10 MPa | Barrel inlet/exit diameter, $D_{barrel}$ | 21 mm |
| Wall thickness safety factor | 3 | Cooling jacket inner diameter | 85 mm |
| Combustion chamber length, $L_c$ | 110 mm | Cooling jacket outer diameter | 100 mm |
| Combustion chamber diameter, $D_c$ | 50 mm | Cooling jacket wall thickness | 7.5 mm |
| Convergent nozzle half-angel, β | 20° | Total heat transfer area, $A_{total}$ | 0.033 m$^2$ |
| Divergent nozzle half-angel, α | 15° | Coolant inlet temperature, $T_i$ | 290 K |
| Throat diameter, $D_t$ | 15 mm | Coolant exit temperature, $T_o$ | 440 K |
| Barrel length, $L_{barrel}$ | 100 mm | Coolant mass flow rate, $\dot{m}_{coolant}$ | 0.4 kg/s |
| | | Total heat transfer rate, $Q_{total}$ | 195.3 kW |

All instrumentation in the HVOF thermal spray system was tested for functionality. Readings on the pressure transducers and thermal-gas/turbine flow meters were verified with calibration charts and calculated values. The ignition system was also run for several conditions to ensure that the spark produced was repeatable. Pressure testing was also done on the system. The line pressures were set to a pressure of 1.5 MPa, at this pressure leaks were detected and repaired in the system as well as the lines to ensure a proper propellants delivery to the gun. During this time, installed pressure transducers also verified their readings and measured 1.5 MPa. After component and leak testing, it was desired to maintain a stable repeatable flame.

Initial experience has been gathered from the hardware previously described to test baseline response and functionality. The operability of all newly developed hardware and software is crucial to the completion of the tests required for this study and needs to be validated. The results of these tests are presented in the following sections as well as lessons learned and proposed changes if any.

# CHAPTER 3: METHODOLOGY

## 3.1- Characterization

### 3.1.1- SCANNING ELECTRON MICROSCOPE (SEM)

The surface morphology is examined using scanning electron microscopy (SEM). The size, shape, and distribution of the particles on the surface, surface texture, and surface morphology can best analyzed using this microscopic method. SEM was employed to look at the interface structures and morphological evolution. SEM has many advantages over traditional microscopes. It has a large depth of field, which allows more of a specimen to be in focus at one time. The SEM also has much higher resolution, so closely spaced specimens can be magnified at much higher levels. Because the SEM uses electromagnets rather than lenses, the researcher has much more control in the degree of magnification. All of these advantages, as well as the actual strikingly clear images, make the scanning electron microscope one of the most useful instruments in research today.

### 3.1.2- X-RAY DIFFRACTION (XRD)

The crystal structure and phase analysis of the coatings is performed using X-Ray Diffraction (XRD). To fully understand the structures of complex alloy coatings, it becomes necessary to understand the local or ultra-microstructures, often arising from structural defects or compositional changes. Local structure of the proposed alloy coating is best studied by grazing incidence x-ray diffraction (GI-XRD). These studies provide information on the atomic scale morphology, crystal structure and phase, and substrate-alloy interface structure of the HVOF coatings. The optimized conditions obtained from the microstructure characterization will be employed to prepare superb coatings for future investigations of thermo-mechanical and thermo-chemical properties.

### 3.1.3- NANOINDENTATION

Nanoindentation obtained the hardness and young's modulus of the coating along with other mechanical properties to determine the effects of velocity, temperature, oxidant content and the degree of melting of particles. Additionally, the test will evaluate which sample has a higher resistance to oxidation and higher material's strength to determine which of the parameters are best to meet the objective of durable coatings for high-temperature and harsh environment.

# CHAPTER 4: RESULTS AND DISCUSSION

## 4.1- Materials Preparation, Treatment, and Analysis

Specimens/substrates (25.4 x 25.4 x 3.175 mm) were first polished using Acetone and then dried immediately. Since the quality assessment was part of this investigation, the surface modification was extremely essential to enhance and improve the adhesion of the coating. Grit blasting was carried out to roughen the surface, which in turn, removed and cleaned any contamination at the surface of the substrate prior to spraying. Moreover, a sufficient enhancement in the bond strength between the deposited coating and substrate surface was resulted by applying the grit blasting to the substrate surface. The girt blasting process was conducted to all specimens using 20 mesh $Al_2O_3$ particles at pressure of 550 kPa to roughen the surface for three minutes. The grid blasted surfaces had roughness on the order of 50 - 60 μm. The specimens were cleaned once more by compressed air prior to apply the desire coating. The HVOF thermal spraying was applied directly after grit blasting process to avoid moisture contamination. A grit blasting machine manufactured by Empire Company was employed to perform the grit blasting process as shown in Fig. 4.1.


Figure 4. 1: Grit blasting machine

## 4.2- Operating and Process Parameters

Several operating and process parameters were tested on substrates. One of the parameters chosen was distance, referring to the length in which the substrate is placed and the tip of the HVOF gun; where the substrate gets hit by the flame with the melting particles of the coating. The second parameter was Mach number which can be distinguished for the exit velocity, pressure chamber and exit temperature. Two different materials for the coatings were used, Inconel 718 and iron aluminide (FeAl), for the purpose of comparing the performance of both coatings.

Three different Mach number conditions of the gas flow were investigated. The particular gas velocities of interest corresponded to Mach numbers of 1, 1.2, and 1.4. The number of distances from the tip of the gun were: 50mm, 100mm and 150mm. However, when the hot firing testing was performed, it was observed that at the distance of 50mm and as the Mach number was increased with each test, the produced coating would fall off the substrate. The reason for such low bonding between the materials was due to a high deposition rate which accumulated until the coating was too thick to adhere properly to the substrate. For this reason, the subsequent data presented would only be for two distances: 100mm and 150mm for Inconel 718. FeAl was sprayed in reduced conditions from the ones of Inconel 718, meaning that not all the parameters were performed for the past coating. Only one distance, 100 mm, and two Mach numbers, 1.0 and 1.2, were done, due to the observation of a decreased coating quality.

Moreover, each sample was subjected to thermal cycling and the data collected for one set of parameters (a specific Mach number with a specific distance) are: a) base sample (no thermal cycling), b) another sample subjected to a temperature of 600°C for 6 hours, and c) a sample that is put under annealing, which was previously subjected to the 600°C and goes into the furnace once again at a temperature of 700°C for 6 hours.

The expected morphology of the particles after spraying are a figure splatted or a particles partially melted with an aura of fully melted material around it making a figure of a sunny up egg

according to (Sidhu et al, 2005). The figure they presented is accurate with the morphology that was found for both materials in all the coatings.

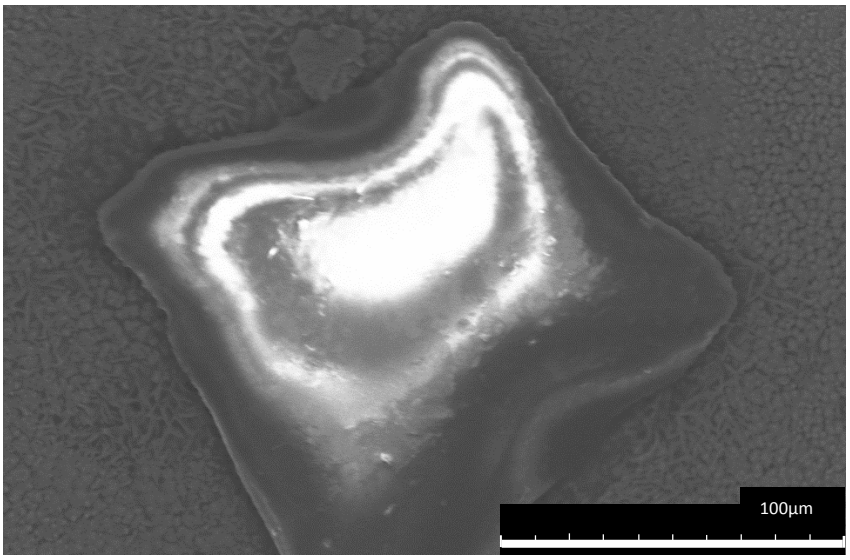


Figure 4.3. Partially melted particle of the HVOF coating after annealing.

Samples were examined using a number of surface analysis techniques. X-Ray Diffraction (XRD) was used to XRD was done in order to obtain all diffraction peaks and phases, so that identifying the phases after the thermal cycling can be compared to the literature and know the oxidation phases, which affect the coating by weakening it.

SEM and XRD go hand in hand, since the crystalline size can be compared and validated with the image of the SEM and the calculations of the XRD. The ideal size of the grains that could be observed would be the smallest grain size after annealing. The reason why the smallest grain size are the most desirable is due to when the coating goes under micro fracture, the crack will go through all the grain until it hits another boundary. The smaller the grain size, the slower the crack fracture will propagate, since it needs to go through the boundary to keep moving. The annealing data is the critical data, since after annealing the grain size grows, and the smallest grain size after all the high temperature process would be an indicative of which process parameter would yield the most desirable results.

For Nanoindentation, the aim was to obtain the two most frequent mechanical properties that are measured using load and depth sensing with the nanoindentation techniques. Those properties are the elastic modulus, E, and the hardness, H. In a very common used technique, data is collected from one complete cycle of loading and unloading. The unloading data is then analyzed according to a model for the deformation of an elastic half space by an elastic punch which relates the contact area at peak load to the elastic modulus (Oliver & Georges, 2004). Techniques for independent estimates of the contact area from the indenter shape function are then used to provide separate measurements of E and H.

## 4.3- Inconel 718

The XRD graphs presented have the same intensity peaks for all the samples, therefore a single graph will be shown (Figure 5.4) for all parameters. For Inconel 718, it is observed that the peaks increase in intensity with increasing annealing temperature since they are in oxidation phase. Such is the case of $Fe_2O_3$ and $Cr_2O_3$, where the peak increases in intensity meaning that the w.t. % of those compounds is increasing. It is observed from the XRD that the peaks tend to sharpen with each annealing as the coating's crystallization is increased via heat addition. The peaks match to those found in literature for Inconel 718 (J.A. Sue, T.P. Chang, 1995). The unoxidized sample shows a diffraction peak at $2\Theta=45^{\circ}$; there is an overlapping of diffraction peaks belonging to $Fe_2O_3$ and Inconel 718 compounds.

The size of the grains can be calculate from the XRD graph, using the Scherrer formula:

$$\tau = \frac{K\lambda}{\beta \cos\theta} \tag{29}$$

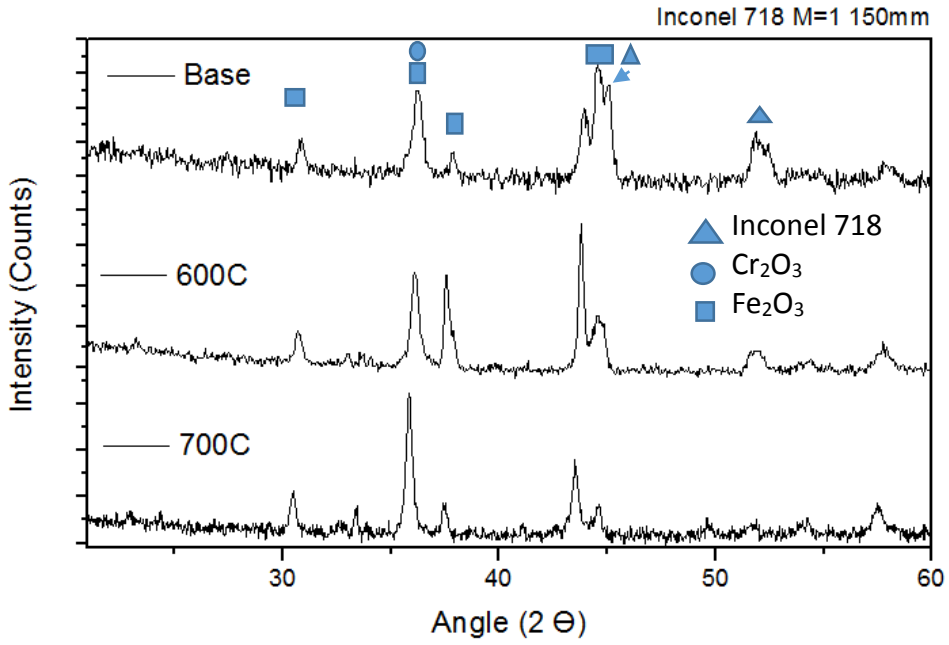


Figure 4.4. XRD graph for Inconel 718**.**

For each individual sample, the crystalline size was calculated through the highest isolated peak, which is located at the 2Θ=35º. The Full width at half maximum (FWHM) was obtained through the analysis software Origin lab, a program that analyses the graph and data obtained from the XRD to calculate different parameters.

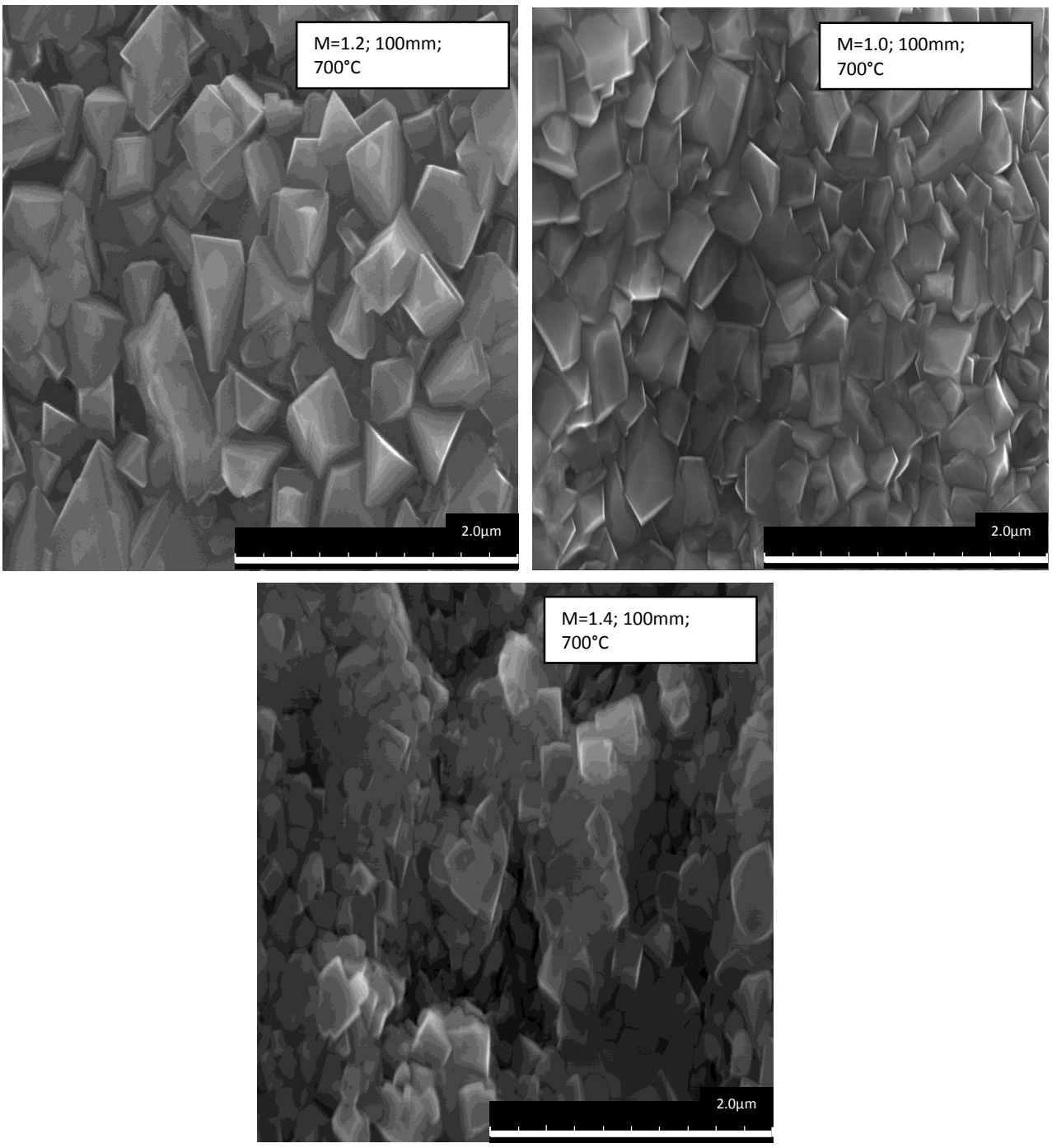


Figure 4.5. SEM images for the fixed parameters 100mm and 700°C, with the different Ma=1, Ma=1.2, Ma=1.4 with a magnification of 25K.

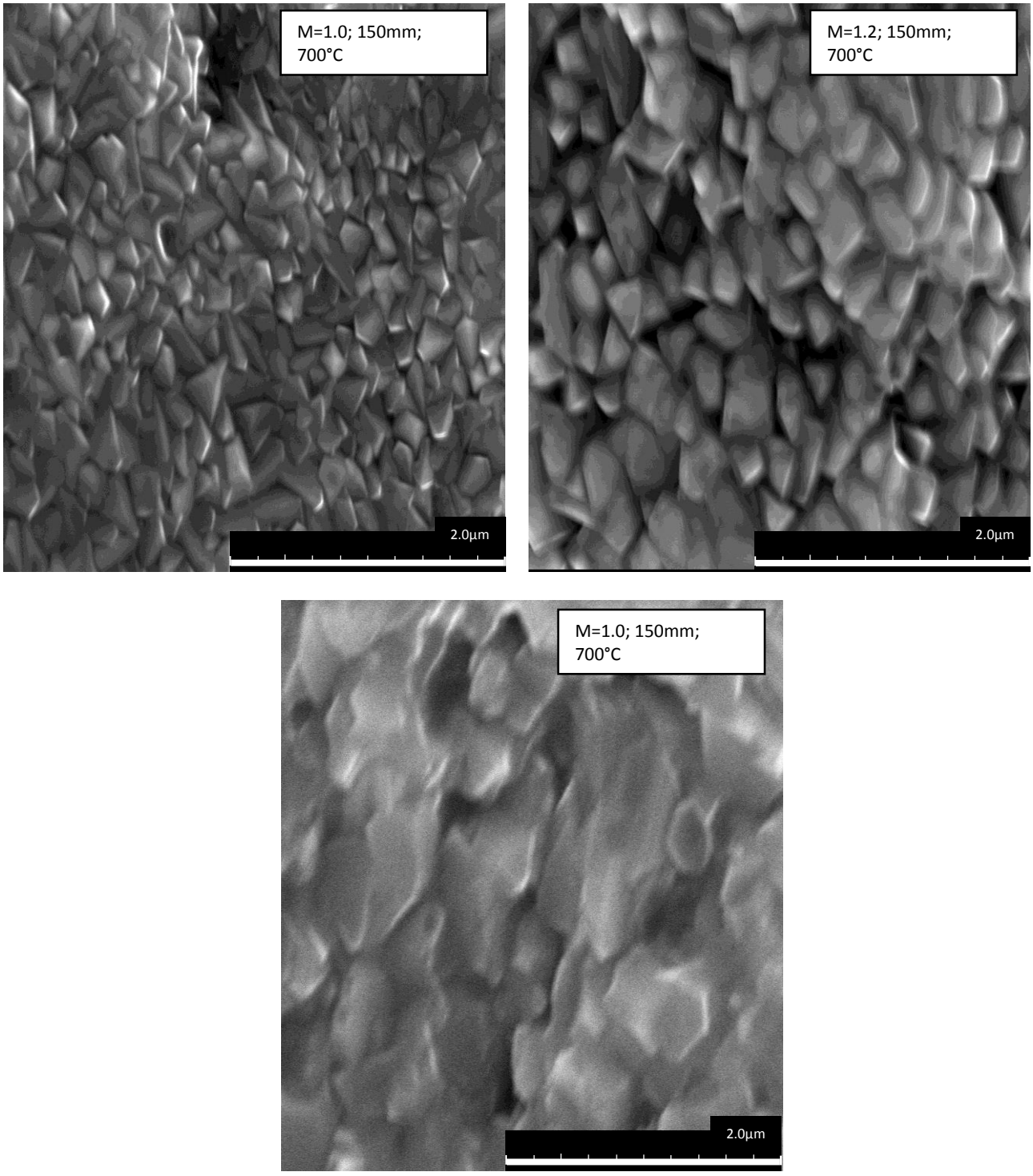


Figure 4.6. SEM images for the fixed parameters 150mm and 700°C, with the different Ma=1, Ma=1.2, Ma=1.4 with a magnification of 25K.

Presented in figures 5.5 and 5.6 are the SEM images side to side to determine which grain size is finer. Estimation of the grain sizes were based on the length scale from the lower right corner of the image. The images that fit the criteria seem to be the third image of figure 4.5 and the first image of figure 4.6. When comparing the calculations for the crystalline size of these two conditions, the finer one comes out to be the one for Ma=1-150mm of 0.4µm as shown in figures 4.5 and 4.6, which is the smallest grain size of all samples.

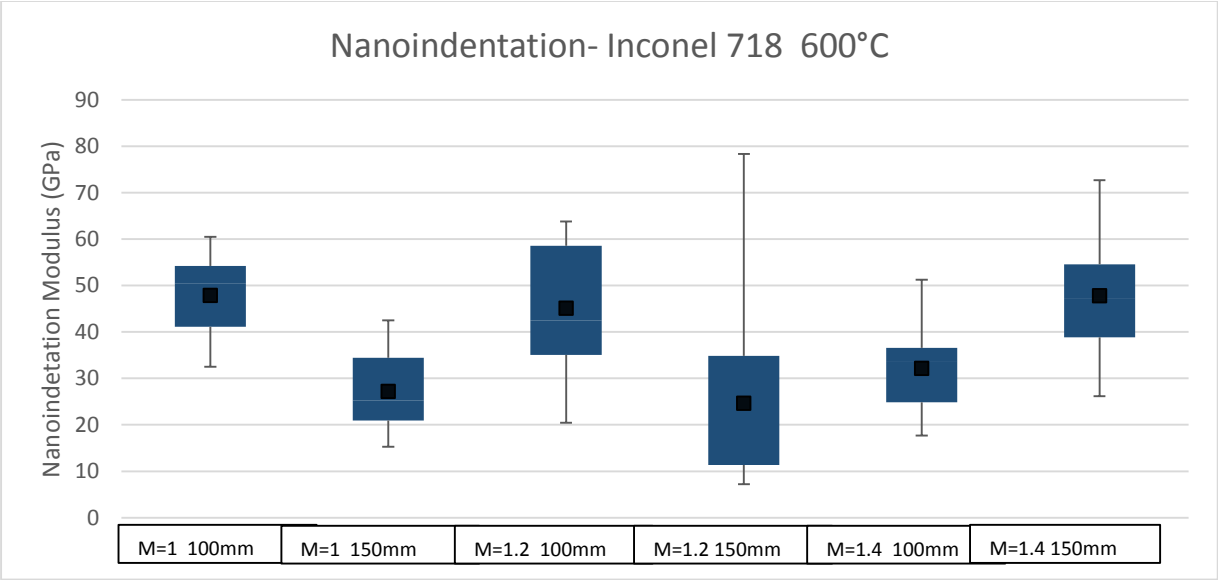


Figure 4.7. Box plot of the data from the nanoindentation at 600°C.

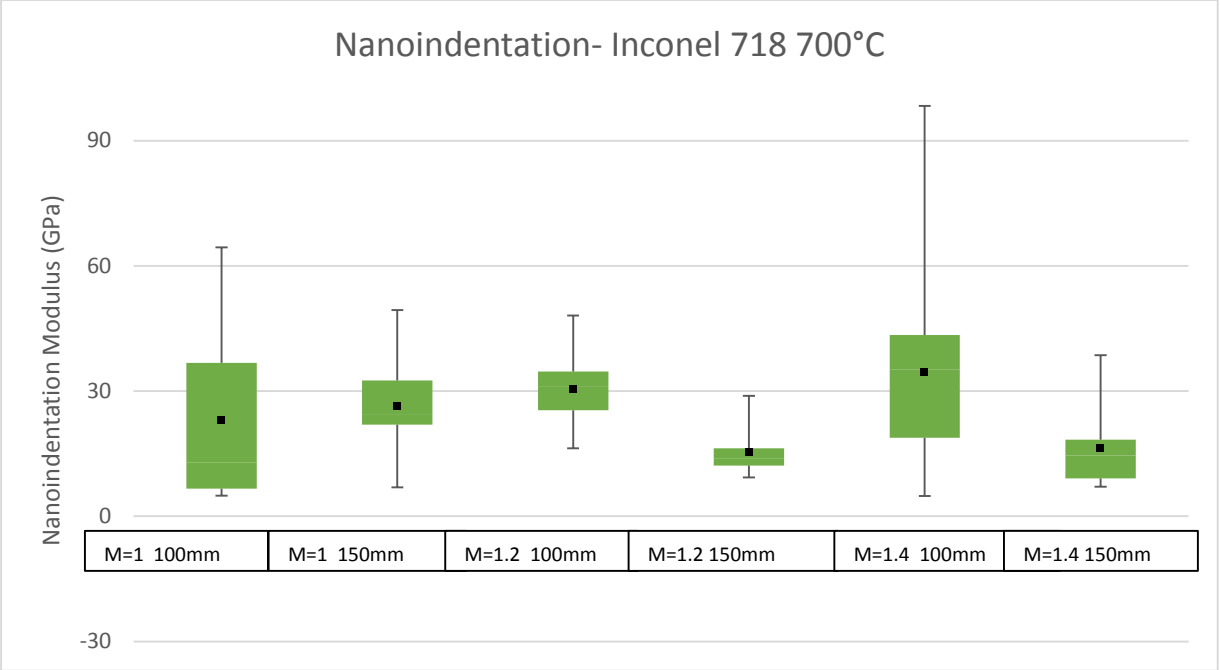


Figure 4.8. Box plot of the data from the nanoindentation at 700°C**.**

Comparing the data obtained and looking for the smallest standard deviation and highest E, the sample that has Ma=1 at 150mm is the best, which is consistent with the sample chosen in the previous sections, as shown in table 4.2.

Table 4.2. Comparison of Mach numbers for the hardness (Inconel 718).

| Temperature | Distance | | | | | |
|---|---|---|---|---|---|---|
| 700°C | M=1 100mm | M=1 150mm | M=1.2 100mm | M=1.2 150mm | M=1.4 100mm | M=1.4 150mm |
| MEAN | 22.924464 | 26.3552423 | 30.4070015 | 15.2589907 | 34.5181716 | 16.2670015 |
| STANDARD DEVIATION | 18.853430 | 10.2991431 | 8.16155873 | 5.02359103 | 21.4562148 | 8.88671102 |

## 4.4- Iron Aluminide

The other material of coating produced was iron aluminide (FeAl) which has a composition of 70% iron and 20% aluminum according to the specifications found in the material sheet provided by Praxair. This material was chosen for its unique qualities of resisting corrosive

environments due to their content of aluminides (Guilemany et al, 2007). No literature source was found to use this exact composition; however at (Guilemany et al, 2007) they used a powder composition of Fe40wt%Al where the sprayed conditions yielded a w.t. % of 70 % for iron. Therefore the data of that investigation will be used to identify the peaks from the XRD of this study's coatings. After thermal cycling, the corrosive product that has a greater presence on the coating is $Fe_2O_3$ (iron oxide) and $Al_2O_3$ (aluminum oxide).

For each individual sample, the crystalline size was calculated through the highest isolated peak, which is located at the 2Θ=33º. The FWHM was obtained through the analysis software Origin lab, a program that analyses the graph and data obtained from the XRD to calculate different parameters.

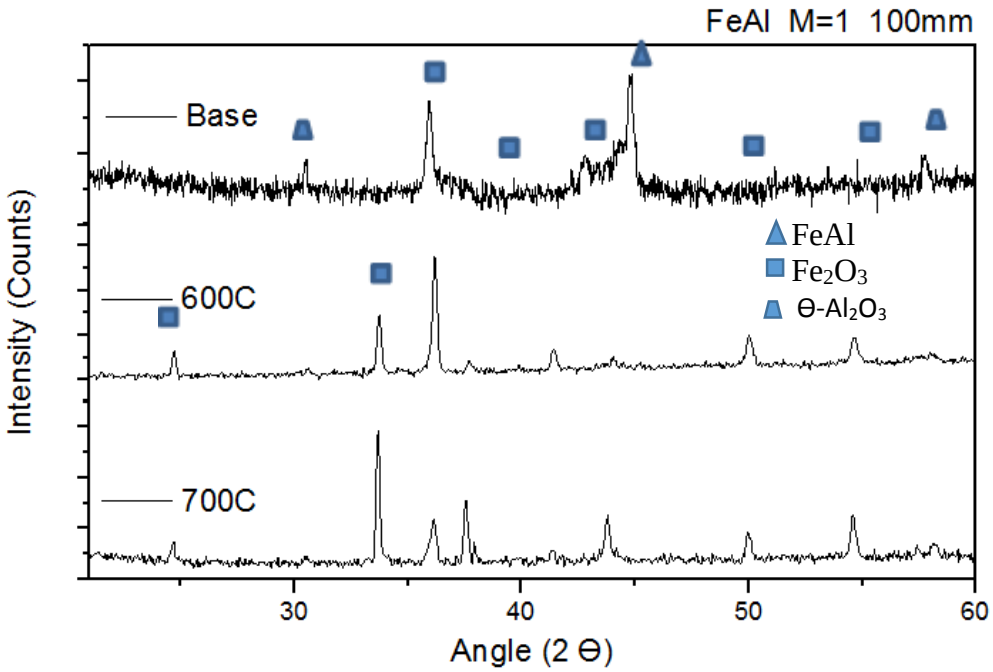


Figure 4.9. XRD graph for Iron Aluminide (FeAl).

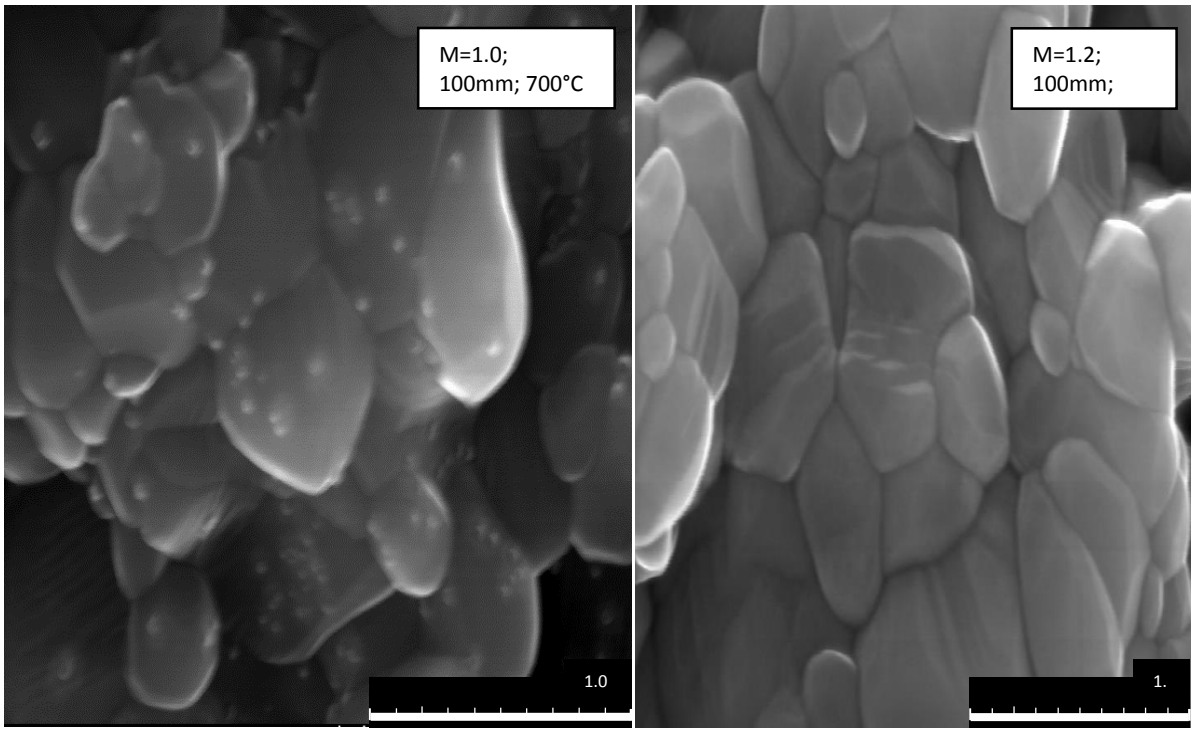


Figure 4.10. SEM images at a scale of 1micrometer and illustrates the different Mach numbers at 700°C.

The SEM images shown side to side in figure 5.10 yield an estimation of the grain sizes of 0.8μm & 0.5μm for the respective pictures. The size were based on the length scale from the lower right corner of the image. The images that fit the criteria seem to be the second image of figure 4.10, corresponding to the Ma of 1.2 for this particular material where the nanoindentation data can be seen in figures 4.11 and 4.12.

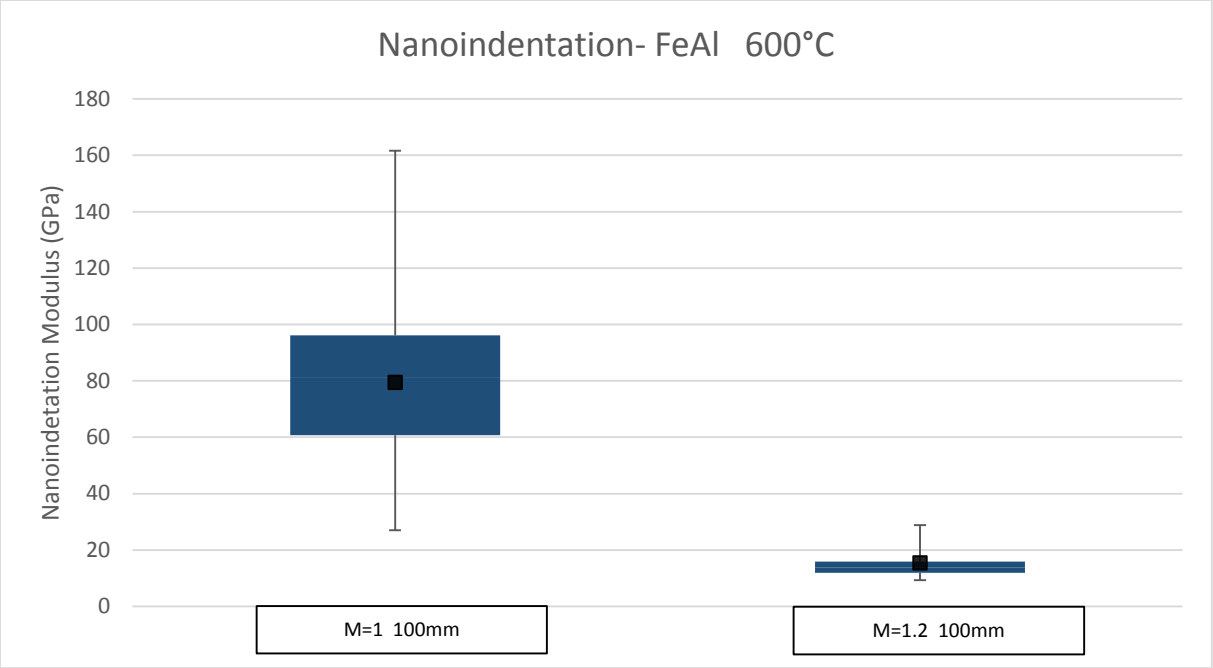


Figure 4.11. Box plot of the data from the nanoindentation at 600°C.

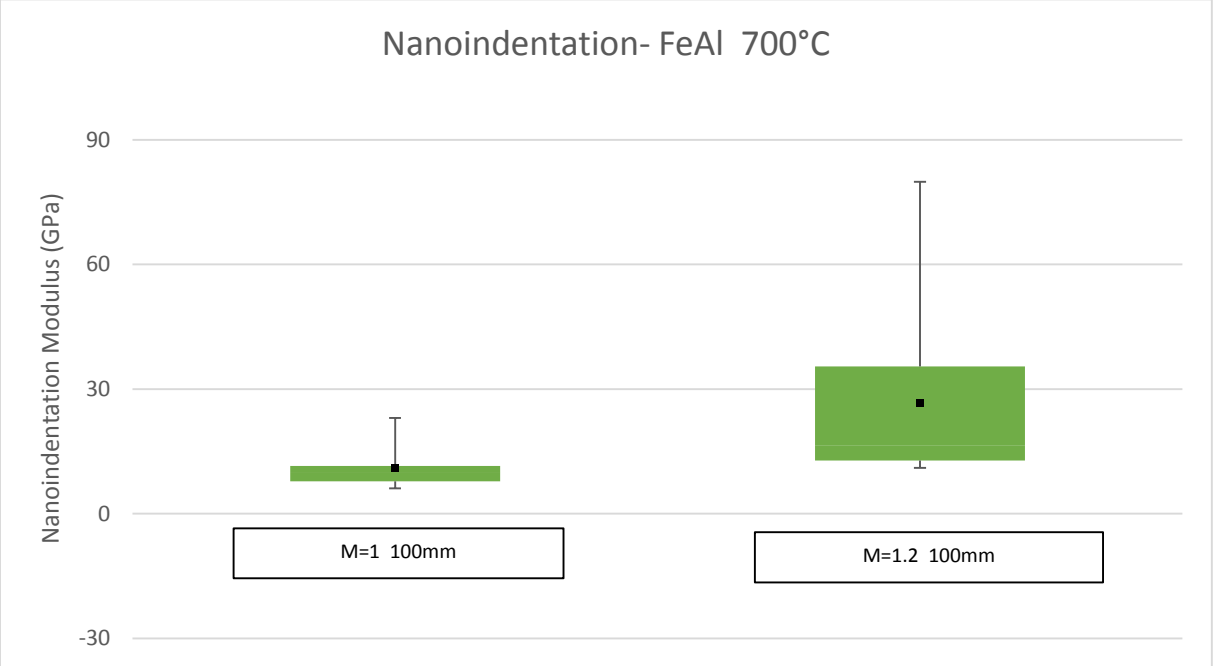


Figure 4.12. Box plot of the data from the nanoindentation at 700°C.

Table 4.3. Comparison of Mach numbers for the hardness (FeAl).

| Temperature | Distance | |
|---|---|---|
| 700°C | M=1<br>100mm | M=1.2<br>100mm |
| MEAN | 15.40904742 | 26.50350668 |
| STANDARD DEVIATION | 5.391693614 | 18.71897761 |

Comparing the data obtained and looking for the smallest standard deviation and highest E, the sample that has Ma=1 is the sample that shows the highest withstanding of loading as shown in table 4.3.

A limitation noticed was that oxidation may have compromised the samples' yield strength (hardness). One of the factors that influenced this result was the time between in which the sample was subjected to thermal cycling and the nanoindentation test.

# CHAPTER 5: CONCLUSION AND FUTURE WORK

A gaseous based HVOF configuration has been developed according to rocket design guidelines. Design was manufactured and assembled with flow monitoring and regulating instrumentation. Setup behavior and flammability ranges have been investigated for a methane-oxygen mixture. Testing revealed initial flaws in lines and remote monitoring arrangements; adequate steps have been taken for the continuous improvement of setup and procedure. Successful tests have shown similar flame shape and oxygen-fuel mixing conditions to industrial HVOF systems with varying exit velocities and overall flow rates. The inclusion of a computational chapter has aided in the understanding of pressure-velocity exchange mechanisms for designed geometry. Additionally, investigation of particle dynamics of gas-fueled HVOF process for a range of operating and process parameters has been done**:** experimental measurements of particle flux and particle velocity at different operating and process parameters were conducted using high speed stereo Particle Image Velocimetry (PIV), while measurements of particle temperature at the same parameters were performed using high speed two color pyrometer. The measured data were compared with the included computational simulation data. The test matrix included testing of:

i. Combustion chamber pressure (200, 275, and 350 kPa)
ii. Total propellants mass flow rate (10, 15, and 20 g/s)
iii. Exit Mach number (1.0, 1.2 and 1.4)
iv. Equivalence ratio ($\phi$) (0.9, 0.95, 1.0, 1.05, and 1.1)
v. Powder feedstock (1.5 and 3 kg/h)
vi. Spraying distance (50, 100 and 150 mm)

Analysis of the coatings were subjected to thermal cycling and then were characterized using SEM, XRD and Nanoindentation. These test were performed to compare the morphologies of each process parameter and study the effect of oxidation on the metallic composites. The ideal coating exhibits the smallest grain size after annealing. The process parameter that yielded such result was Ma 1.2 at 150mm. It was observed that the time between the oxidation may have compromised the samples' yield strength (hardness). One of the factors that influenced this result was the time between in which the sample was subjected to thermal cycling and the nanoindentation test.

Future work objectives are as follows:

a) **The next generation of coatings** produced should be fabricated at the Ma number that yielded the lowest grain size obtained from the results of this report, Ma 1.2. The test matrix for distances should start at 150 mm from the tip of the gun, since at this specific distance the grain sizes were lower than the ones found at 100mm. Moreover, the time between the thermal cycling and the nanoindentation should be as low as possible due to the impact of oxidation in the samples.

b) **Continuous setup improvement and transition into liquid:** as evidenced in the conclusions, the testing setup must be always in the process of redesigning and reconfiguring to achieve the optimal operation of the experimental procedure. Although only one parameter must be changed per objective to properly correlate results with variations, the setup is expected to be able to alter one mechanism at a time until a completely new design is obtained. A liquid-gas combustion must be performed sometime in the future in order to compare the coatings produced by gaseous HVOF system to it. Finally, a system redesign may be able to take place to accommodate components that

cannot be integrated in the current setup (internal thermocouples, pressure sensing device inside the combustion chamber) and/or fulfill a different design approach.

# References


*Advance Surface Technology*. (2008). Retrieved from www.surfacetechno.com

Al-Shehri, Y. A. (2011). *Mechanical and Metallurgical Properties of Two-Layered Diamalloy 4010 and 2002 HVOF Coating.* Dublin City University.

B. Hwang, S. L. (2001). Correlation of microstructure and wear resistance of molybdenum blend coating fabricated by atmospheric plasma spraying. *Material Science and Engineering, 3*, 152- 163.

B. Wielage, A. W. (2006). Development and Trends in HVOF Spraying Technology. *Surface & Coating Technology, 6*, 2032-2037.

Bach FW, M. K. (2004). Particle Image Velocimetry in Thermal Spraying. *Materials Science and Engineering, 1a*, 146–152.

Bach, F., Mohwald, K., Engl, L., Drobler, E., & Hartz, K. (2006). Particle Image Velocimetry in Thermal Spraying. *Advanced Engineering Materials*, 650-653.

Basu, S., & Cetegen, B. M. (2008). Modeling of liquid ceramic precursor droplets in a high velocity oxy-fuel flame jet. *Acta Materialia, 56*, 2750-2759.

C.N. Machio, G. A. (2005). Performance of WC-VC-Co thermal spray coating in Abrasion and slurry erosion tests. *Wear, 5*, 434-442.

Cheng D, T. G. (2003). Mathematical modeling of high velocity oxygen fuel thermal spraying of nano crystalline materials: an overview. *Modeling and Simulation in Materials Science and Engineering, 8*.

Cheng D, X. Q. (2001). A numerical study of high-velocity oxygen fuel thermal spraying process Part I: gas phase dynamics. *Metallurgical and Materials Transactions, 75*, 1609–1620.

D. Stewart, P. S. (1998). Influence of heat treatment on the abrasive wear behavior of HVOF sprayed WC-Co coatings. *Surface and Coatings Technology, 32*, 13-24.

Dolatabadi A, M. J. (2003). Effect of a cylindrical shroud on particle conditions in high velocity oxy-fuel (HVOF) spray process. *Journal of Materials Processing Technology, 23*, 214–224.

Dongmo E, W. M. (2008). Analysis and Optimization of the HVOF Process by Combined Experimental and Numerical Approaches. *Surface & Coatings Technology, 76*, 4470–4478.

Dongmo, E., Wenzelburger, M., & Gadow, R. (2008). Analysis and optimization of the HVOF process by combined experimental and numerical approaches. *Surface & Coatings Technology*, 4470-4478.

Dynalene, C. (n.d.). *Dynalene Selection Guide*. Retrieved from http://www.dynalene.com/Fluid-selection-guide-s/1828.htm

G.Reisel, B. W. (2001). High temperature oxidation behavior of HVOF-Sprayed unreinforced and reinforced molybdenum disilicida powders. *Surface and Coatings Technology, 63*, 19-26.

Goulaouen, G. (1998). Influence of Spray Parameters on Stainless Steel Coating Properties. *Proceeding of the 15th ITS*, 537-545.

Gourlaouen, G. (1998). Influence of Spray Parameters on Stainless Steel Coating Properties. *Proceeding of the 15th ITS, 31*, 537-545.

Gu S, E. C. (2001). Computational fluid dynamic modeling of gas flow characteristics in a high-velocity oxy-fuel thermal spray system. *Journal of Thermal Spray Technology, 12*, 461–469.

Guilemany, J.M., Cinca, N., Dosta, S., and Lima, C.R.C. (2007), High-temperature oxidation of Fe40Al coatings obtained by HVOF thermal spray, *Intermetallics*, Volume 15, Issue 10, Pages 1384-1394.

H.Y. Al-Fadhli, J. S. (2006). The erosion-corrosion behavior of high velocity oxy-gen fuel (HVOF) thermally sprayed inconel-625 coatings on different metallic surfaces. *Surface & Coating Technology, 14*, 5782-578.

Hassan B, O. W. (1995). Computational fluid dynamic analysis of a high velocity oxygen-fuel (HVOF) thermal spray torch. *Thermal Spray Science and Technology, 54*, 193–198.

Heath GR, H. P. (1997). An Assessment of Thermal Spray Coating Technologies for High Temperature Corrosion Protection. *Materials Science Forum, 57*, 809-816.

Huzel, D. a. (1992). *Modern Engineering for Design of Liquid Propellant Rocket Engines.*

J. Tan, L. M. (1999). Component Repair using HVOF thermal spraying. *Journal of Materials Processing Technology, 47*, 203-208.

J.M. Guliemany, J. F. (2002). Effects of thickness coating on the electrochemical behavior of thermal spray Cr3C2-NiCr coatings. *Surface & Coating Technology, 75*, 107-113.

Jang HJ, P. D. (2006). Mechanical Characterization and Thermal Behavior of HVOF-Sprayed Bond Coat in Thermal Barrier Coatings (TBCs). *Surface & Coatings Technology* , 4355 – 4362.

Jang, H. P. (2006). Mechanical characterization and thermal behavior of HVOF-sprayed bond coat in thermal barrier coatings (TBCs). *Surfaace & Coatings Technology, 58*, 4355-4362.

Jang, H., Park, D., Jung, Y., Jang, J., Choi, S., & Paik, U. (2006). Mechanical characterization and thermal behavior of HVOF-sprayed bond coat in thermal barrier coatings (TBCs). *Surfaace & Coatings Technology, 200*, 4355-4362.

K. Padilla, A. V. (2002). Fatigue Behavior of 4140 Steel coated with a NiMoAl deposit Applied by HVOF Thermal Spray. *Surface & Coating Technology, 21*, 151-162.

Kamali, R., & Binesh, A. (2009). The importance of sensitive parameters effect on the combustion in a high velocity oxygen-fuel spray system. *International Communications in Heat and Mass Transfer*, 978-983.

Kamnis S, G. S. (2005). Numerical modelling of propane combustion in a high velocity oxygen fuel thermal spray gun. *Chemical Engineering and Processing: Process Intensification, 74*, 246–253.

Kamnis S, G. S. (2008). Mathematical modelling of Inconel 718 particles in HVOF thermal spraying. *Surface & Coatings Technology, 35*, 2715–2724.

Kamnis, S., & Gu, S. (2006). 3-D Modelling of kerosene-fuelled HVOF thermal spray gun. *Chemical Engineering Science*, 5427-5439.

Katanoda H, M. H. (2011). Experimental and Numerical Evaluation of the Performance of Supersonic Two-Stage High-Velocity Oxy-Fuel Thermal Spray (Warm Spray) Gun. *Journal of Thermal Science*, 88-92.

Katanoda, H. M. (2011). Experimental and Numerical Evaluation of the Performance of Supersonic Two-Stage High-Velocity Oxy-Fuel Thermal Spray (Warm Spray) Gun. *Journal of Thermal Science, 73*, 88-92.

Katanoda, H., Morita, H., Komatsu, M., & Kuroda, S. (2011). Experimental and Numerical Evaluation of the Performance of Supersonic Two-Stage High-Velocity Oxy-Fuel Thermal Spray (Warm Spray) Gun. *Journal of Thermal Science, 20*(1), 88-92.

Kawakita J, K. S. (2006). Dense Titanium Coatings by Modified HVOF Spraying. *Surface & Coatings Technology, 86*, 1250–1255.

L. Fedrizzi, S. R. (2004). Bonora, Corrosion and wear behavior of HVOF cermet coatings Used to replace hard chromium Electrochimica Acta. *35*, 2803-2814.

L. Zhoa, M. M. (2004). Influence of spray parameters on the particle in-flight properties and the properties of HVOF coating of WC-CoCr. *Wear, 36*, 41-46.

Li M, C. P. (2003). Modeling and analysis of HVOF thermal spray process accounting for powder size distribution. *Chemical Engineering Science, 35*, 849-857.

Li, M., & Christofides, P. (2005). Multi-scale modeling and analysis of an industrial HVOF thermal spray process. *Chemical Engineering Science*, 3649-3669.

Lillo, T., & Wright, R. (2008, July). Microstructure, Processing, Performance Relationships for High Temperature Coatings. In *22nd Annual Conference on Fossil Energy Materials*.

Lim, Y. W. (2007). Tribological behavior of nanostructured WC particles/polymer coatings. *wear, 65*, 1097-1101.

Lim., Y. W. (2007). Tribological behavior of nanostructured WC particles/polymer coatings. *wear, 69*, 1097-1101.

Lopez AR, H. B. (1998). Computational fluid dynamics analysis of a wire-feed, high-velocity oxygen fuel (HVOF) thermal spray torch. *Journal of Thermal Spray Technology, 67*, 374–382.

M, B. S. (2008). Modeling of Liquid Ceramic Precursor Droplets in a High Velocity Oxy-fuel Flame Jet. *Acta Materialia, 74*, 2750–2759.

M. Hasan, J. S. (2008). Effect of spray parameters on residual stress build-up of HVOF sprayed aluminum/toolsteel functionally graded coatings. *Surface & Coating Technology, 63*, 4006-4010.

Marple, R. L. (2003). Optimized HVOF Titania Coatings. *Journal of Thermal Spray Technology, 32*, 360-369.

Metco, S. (2012). *High Velocity Oxy-Fuel (HVOF) Solutions.* Switzerland.

Mostaghimi J, C. S.-A. (2003). Modeling thermal spray coating processes: a powerful tool in design and optimization. *Surface and Coatings Technology, 67*, 1–11.

O, S. G. (2010). *Rocket Propulsion Elements.*

Oberkampf WL, T. M. (1996). Analysis of a high velocity oxygen fuel (HVOF) thermal spray torch Part 1: numerical formulation. *Journal of Thermal Spray Technology, 24*, 53–61.

Oberkampf WL, T. M. (1996). Analysis of a high velocity oxygenfuel (HVOF) thermal spray torch Part 2: computational results. *Journal of Thermal Spray Technology, 63*, 62–68.

Oksa, M., Turunen, E., T, S., Varis, T., & and Hannula, S. (2011). Optimization and Characterization of High Velocity Oxy-fuel Sprayed Coatings: Techniques, Materials, and Applications. *Coatings, 52*, 17-52.

Oliver, W. C., & Pharr, G. M. (2004). Measurement of hardness and elastic modulus by instrumented indentation: Advances in understanding and refinements to methodology. *Journal of materials research*, Volume *19, No.* 1, Pages 3-20.

P. Gao, C. L. (2008). Influence of substrate hardness on deposition behavior of single porous WC-12Co particle in cold spraying. *Surface and Coatings Technology, 84*, 384-390.

Power GD, S. E. (1991). Analysis of a combustion (HVOF) spray deposition gun. *UTRC, 73*, Report No. 91-8.

S, K. S. (2006). 3-D Modelling of Kerosene-fuelled HVOF Thermal Spray Gun. *Chemical Engineering Science, 51*, 5427 – 5439.

S. Kuroda, Y. T. (2001). Peening Action and Residual Stresses in High Velocity Oxygen Fuel Thermal Spraying of 316L Stainless Steel. *Journal of Thermal Spray Technology, 41*, 367-374.

Sidhu TS, P. S. (2005). Studies on The Properties of High Velocity Oxy-fuel Thermal Spray Coatings for Higher Temperature Applications. *Materials Science, 43*, 805-823.

Sidky P.S., & Hocking, M.G. (1999). Review Of Inorganic Coatings And Coating Processes For Reducng War And Corrosion. *Brit. Corr. J., 34*, No. 3, 171-183.

Smith EB, P. G. (1992). Application of computational fluid dynamics to the HVOF thermal spray gun. *ASM International, 23*.

Sobolev V.V., Guilemany, J.M., Nutting, J. (2004). HVOF Spraying, B0655, Maney, IOM3

Sue, J.A., Chang, T.P. (1995), Friction and wear behavior of titanium nitride, zirconium nitride and chromium nitride coatings at elevated temperatures, *Surface and Coatings Technology*, Volumes 76–77, Part 1, Pages 61-69.

Sutton, G. (2005). *History of Liquid Propellant Rocket Engines.*

Swank WD, F. J. (1994). HVOF gas flow field characteristics. *Proceedings of the Seventh National Thermal Spray Conference, 73*, 313–318.

T.C. Totemeier, R. W. (2002). Microstructure and stresses in HVOF Sprayed Iron Aluminide Coatings. *Journal of Thermal Spray Technology, 36*, 400-408.

T.C. Totemeier, R. W. (2003). Mechanical and Physical Properties of High-VelocityOxy-Fuel-Sprayed Iron Aluminide Coatings. *Metallurgical and material Transactions A, 42*, 2223-223.

T.C. Totemeier, R. W. (2004). Residual Stresses in High Velocity Oxy-Fuel Metallic Coatings. *Metallurgical and material Transactions, 36*, 1807-1814.

Tabbara H, a. G. (2009). Computational Simulation of Liquid-fuelled HVOF Thermal Spraying. *Surface & Coatings Technology, 41*, 676–684.

Tabbara, H., & Gu, S. (2009). Computational Simulation of liquid-fuelled HVOF thermal spraying. *Surface & Coatings Technology*, 676-684.

Tang F, A. L. (2004). Characterization of Oxide Scales Formed on HVOF NiCrAlY Coatings with Various Oxygen Contents Introduced During Thermal Spraying. *Scripta Materialia, 68*, 25–29.

V. Stoica, R. A. (2004). Silding Wear Evaluation of Hot Isostatically Pressed Thermal Spray Cermet Coatings. *Journal of Thermal Spray Technology, 74*, 93-107.

W. Hu, M. L. (2008). Preparation and properties of HVOF NiAl nanostructured coatings. *Material Science and Engineering A, 56*, 1-8.

W.C. Lih, S. Y. (2000). Effects of process parameters on molten particle speed and surface temperature and the properties of HVOF CrC/NiCrcoating. *Surface and Coatings Technology, 52*, 54-60.

W.J. Trompetter, A. M. (2002). Role of oxides in high velocity thermal spray coatings. *Nuclear Instruments and Methods in Physics Research B, 36*, 518-523.

Y. Qiao, T. F. (2003). The effects of fuel chemistry and feed stock powder structure on the mechanical and tribological properties of HVOF thermal-sprayed WC-Co coatings with very fine structures. *Surface and Coatings Technology, 43*.

Yang V, H. M. (2005). *Liquid Rocket Thrust Chambers.*

Yang X, a. E. (1996). Numerical analysis of the high velocity oxygen–fuel (HVOF) thermal spray (TS) system. *J. Therm. Spray Technol, 17*, 175–184.

Zeoli N, G. S. (2008). Numerical simulation of in-flight particle oxidation during thermal spraying. *Comput. Chem. Eng., 18*.

Zhang D, H. S. (2003). Microstructure formation and corrosion behavior in HVOF-sprayed Inconel 625 coatings. *Material Science Engineering, 57*, 45–56

# Vita

This thesis was written by Ana Cecilia Rios Ibanez, a student with a Bachelors in Mechanical Engineering and by the end of the submission of this paper, a Masters in Mechanical Engineering. Rios lives in two cities with two humans and two dogs. Rios works as a graduate student in the University of Texas at El Paso's Center of Space Exploration and Technology Research (cSETR) within projects of the Department of Energy.

Contact Information: acrios2@miners.utep.edu

This thesis/dissertation was typed by Ana Cecilia Rios Ibanez